Novel Insight into Microbially Mediated Nitrate-Reducing Fe(II) Oxidation by *Acidovorax* sp. Strain BoFeN1 Using Dual N−O Isotope Fractionation

Dandan Chen,[○] Kuan Cheng,[○] Tongxu Liu, Guojun Chen,* Andreas Kappler, Xiaomin Li, Raymond Jianxiong Zeng, Yang Yang, Fujun Yue, Shiwen Hu, Fang Cao, and Fangbai Li

Cite This: *Environ. Sci. Technol.* 2023, 57, 12546−12555

Read Online

ACCESS | Metrics & More | Article Recommendations | Supporting Information

ABSTRACT: Microbially mediated nitrate reduction coupled with Fe(II) oxidation (NRFO) plays an important role in the Fe/N interactions in pH-neutral anoxic environments. However, the relative contributions of the chemical and microbial processes to NRFO are still unclear. In this study, N−O isotope fractionation during NRFO was investigated. The ratios of O and N isotope enrichment factors $(^{18}\varepsilon{:}^{15}\varepsilon)$-$NO_3^-$ indicated that the main nitrate reductase functioning in *Acidovorax* sp. strain BoFeN1 was membrane-bound dissimilatory nitrate reductase (Nar). N−O isotope fractionation during chemodenitrification [Fe(II) + NO_2^-], microbial nitrite reduction (cells + NO_2^-), and the coupled process [cells + NO_2^- + Fe(II)] was explored. The ratios of $(^{18}\varepsilon{:}^{15}\varepsilon)$-$NO_2^-$ were 0.58 ± 0.05 during chemodenitrification and -0.41 ± 0.11 during microbial nitrite reduction, indicating that N−O isotopes can be used to distinguish chemical from biological reactions. The $(^{18}\varepsilon{:}^{15}\varepsilon)$-$NO_2^-$ of 0.70 ± 0.05 during the coupled process was close to that obtained for chemodenitrification, indicating that chemodenitrification played a more important role than biological reactions during the coupled process. The results of kinetic modeling showed that the relative contribution of chemodenitrification was 99.3% during the coupled process, which was consistent with that of isotope fractionation. This study provides a better understanding of chemical and biological mechanisms of NRFO using N−O isotopes and kinetic modeling.

KEYWORDS: *nitrate-reducing Fe(II) oxidation, nitrite reduction, N and O isotope fractionation, chemical and microbial processes, cell encrustation*
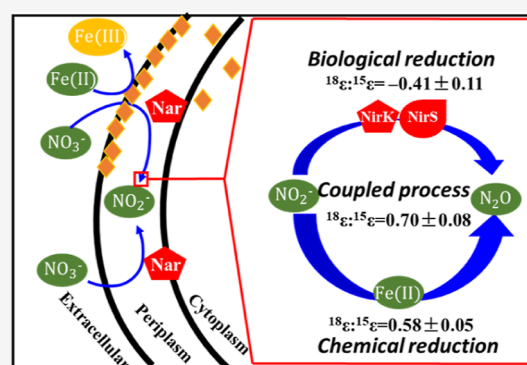
1. INTRODUCTION

Redox transformations of Fe and N, which can be microbially and chemically mediated by nitrate-reducing Fe(II) oxidation (NRFO) bacteria, are important geochemical processes in the environment.[1,2] Microbial nitrate reduction is a major natural N-cycling process that controls the concentration of nitrate in natural or engineered water systems. Fe(II) oxidation during NRFO can cause the formation of Fe(III) minerals,[3] resulting in the immobilization of heavy metal pollutants (e.g., Cd, Cr, and As) and the stabilization of soil organic carbon.[4−6]

N−O isotope fractionation was suggested to be a powerful tool for investigating the microbially mediated NRFO processes.[7−10] During dissimilatory nitrate and nitrite reduction, lighter isotopes (e.g., ^{14}N and ^{16}O) react faster than heavier isotopes (e.g., ^{15}N and ^{18}O).[11] Normal isotope effects cause the heavier isotopes to accumulate in the remaining substrate, whereas the lighter ones are enriched in the product.[11] Changes in isotope fractionation of the reactant might, therefore, provide evidence as an "isotopic fingerprint" of ongoing microbial or chemical nitrate transformation,

whereas diffusion or dilution causes little isotope fractionation.[7] The ratio of the O and N isotope enrichment factors $(^{18}\varepsilon{:}^{15}\varepsilon)$-$NO_3^-$ was close to 1.0 with membrane-bound dissimilatory nitrate reductase (Nar),[12−14] whereas it was 0.4−0.7 for bacteria with periplasmic dissimilatory nitrate reductase (Nap).[7,12−15] Therefore, $^{18}\varepsilon{:}^{15}\varepsilon$ provides a reliable baseline for distinguishing Nar from Nap. Chen et al. (2020) identified the type of nitrate reductase during NRFO by *Pseudogulbenkiania* sp. strain 2002,[7] which contains the genes of both *narG* and *napA*. The $(^{18}\varepsilon{:}^{15}\varepsilon)$-$NO_3^-$ ratios of 0.45−0.69 indicate that Nap was mainly expressed under their experimental conditions.[7] The investigations of nitrate

reductase for other typical NRFO bacteria using N and O isotopes are needed.

NRFO bacteria face the challenge of precipitating poorly soluble Fe(III) minerals, which might precipitate on the cell surface, in the periplasm and cytoplasm and result in cell encrustation.[16] Cell encrustation can impair the cellular uptake of nutrients and substrates, limit metabolic activity, and finally lead to cell death and lysis.[17] Cell encrustation can also modify bacterial physiological states and affect mass-transfer processes prior to bond cleavage, resulting in isotope variations.[7] Nitrate reduction rates and metabolic state in NRFO bacteria (e.g., strain 2002) are substantially suppressed by cell encrustation, whereas another type of NRFO bacteria (e.g., *Acidovorax* sp. strain BoFeN1) generates extracellular polymeric substances (EPSs) around the cells to shield them against encrustation and maintain metabolic activity.[18,19] To date, limited knowledge is available about the effects of cell encrustation and Fe(II) oxidation on N and O isotope fractionation during NRFO by these bacteria.

During NRFO, dissimilatory nitrate is reduced to nitrite, and nitrite is further reduced through nitrite reductase. Meanwhile, nitrite can be chemically reduced by Fe(II) as well. Thus, biological and chemical nitrite reductions coexist during NRFO. Kinetic modeling is a useful tool for assessing the contributions of microbial and chemical nitrite reduction during NRFO.[7,19] Liu et al. (2019)[19] suggested that biological nitrite reduction was the main process, whereas Chen et al. (2020)[7] suggested that chemical reaction was the major process during NRFO. Therefore, the primary processes involved in NRFO remain unclear. N and O isotope fractionation is a promising method for distinguishing between biological and chemical processes during NRFO.[8] Copper-containing nitrite reductase (NirK) and cytochrome cd1-containing nitrite reductase (NirS) were identified as two dissimilatory nitrite reductase. N and O isotope fractionation of microbial nitrite reduction by these two families of enzymes was different.[20] The ratio of $(^{18}\varepsilon:^{15}\varepsilon)$-$NO_2^-$ was about 0.75 for the three strains with NirS (*Pseudomonas aeruginosa*, *Pseudomonas chlororaphis*, and *Pseudomonas stutzeri*), whereas that was nearly 0.09 for the three strains with NirK (*Pseudomonas aureofaciens*, *Achromobacter xylosoxidans*, and *Ochrobactrum* sp. strain 3CB4). For chemodenitrification, a variety of environmental effects [e.g., temperature, nitrite/Fe(II) concentrations, and different coexisting minerals] on N and O isotope fractionation have been investigated.[8,21−23] However, a direct comparison of the $(^{18}\varepsilon:^{15}\varepsilon)$-$NO_2^-$ ratios for chemodenitrification, microbial nitrite reduction, and the coupled process during NRFO is still lacking.

In this study, the strain BoFeN1 was chosen as the model strain. The kinetics, cell encrustation, and N−O isotope fractionation of NRFO were thoroughly examined. This study aimed to (1) investigate the impact of cell encrustation on kinetics and N−O isotope fractionation during nitrate reduction, (2) identify nitrate reductase using the ratio of $(^{18}\varepsilon:^{15}\varepsilon)$-$NO_3^-$, and (3) distinguish chemical from biological processes during NRFO by N−O isotopes and a kinetic model.

2. MATERIALS AND METHODS

2.1. Culturing. An oxygen-free, 30 mM piperazine-*N,N′*-bis (2-ethanesulfonic acid) (PIPES)-buffered freshwater mineral medium (pH 7.0) was used to culture the strain BoFeN1. The freshwater mineral medium contained (per liter) 0.3 g of NaCl, 0.3 g of NH₄Cl, 0.42 g of MgCl₂·6H₂O, 0.14 g of KH₂PO₄, 0.1 g of CaCl₂·2H₂O, 10 mL of vitamin solution, and 10 mL of trace element solution.[24] As the electron donor and acceptor, 10 mM sodium acetate and 8 mM sodium nitrate were added to the medium to prepare the cell suspension. The bacteria were anaerobically grown to the early stationary growth phase, extracted by centrifugation (6000g, 24 °C) for 10 min, washed twice in anaerobic PIPES buffer (100% nitrogen atmosphere), and then resuspended in a sterile serum bottle to provide cell suspension for the subsequent experiments. The cell suspension was flushed with N₂ for at least 40 min, sealed with butyl stoppers, and crimp-sealed.

2.2. Experimental Design. The 58 mL serum bottles with 20 mL of medium containing only the PIPES buffer and electrolyte [e.g., NaNO₃, NaNO₂, sodium acetate, and Fe(II)] were used for all studies. Five different treatments were conducted as follows: cells + NO_3^- + Fe(II), cells + NO_3^-, cells + NO_2^- + Fe(II), NO_2^- + Fe(II), and cells + NO_2^-. The bottles were filled with medium buffered with 30 mM PIPES, and the pH was changed to 7.0. The bottles were sealed using butyl rubber stoppers and crimped. After autoclaving the bottles at 121 °C for 20 min, Fe(II), sodium acetate, sodium nitrate, and sodium nitrite were added in the glovebox [Plas-Labs, USA, H₂/N₂ (1/99, v/v)]. The initial concentrations of Fe(II), nitrate, nitrite, and sodium acetate were 5 mM, with 5 × 10⁸ cells mL⁻¹ of strain BoFeN1. Each experiment was carried out in triplicate and incubated in the dark at 30 °C.

2.3. Chemical and Stable Isotope Analysis. Concentrations of nitrate, nitrite, N₂O, Fe(II), and acetate were quantified. The concentration of N₂O was measured using a Techcomp GC7900 gas chromatograph equipped with an ECD detector. Ion chromatography (DionexICS-90) with an anion-exchange column (IonPac AS14A, 4 × 250 mm) was used to measure the concentrations of NO_3^-, NO_2^-, and acetate. The concentration of NH_4^+ was measured via a continuous-flow analyzer (SAN++, Skalar).[25] The Fe(II) concentration was determined using the 1,10-phenanthroline method.[19] Transmission electron microscopy (TEM, JEM-2011, JEOL) and X-ray diffraction (XRD, D2 phaser, Bruker) were used to investigate the cell encrustation and structure of the formed minerals.

The $\delta^{15}N$ and $\delta^{18}O$ values of nitrate and nitrite {where $\delta^{15}N = [(^{15}N/^{14}N)_{sample}/(^{15}N/^{14}N)_{standard} - 1] \times 1000$ (‰) and $\delta^{18}O = [(^{18}O/^{16}O)_{sample}/(^{18}O/^{16}O)_{standard} - 1] \times 1000$ (‰)} were quantified using the azide method following McIlvin and Altabet (2005).[26] NO_2^- was removed by sulfamic acid prior to N and O isotopic analysis of NO_3^-. The samples were treated with 0.5 mL of 1.0 M sulfamic acid (Macklin, Shanghai, China) for 15 min. The extract solutions were neutralized with 0.5 mL of 1.0 M NaOH. NO_3^- was first reduced to NO_2^- by cadmium powder for 8 h, and then NO_2^- was converted to N₂O by sodium azide for 2 h. The NO_3^- or NO_2^- sample was diluted to approximately 1.43×10^{-5} M (N) with 0.5 M NaCl, and then 5 mL of the diluted sample was withdrawn into a 15 mL centrifuge tube. The pH value was adjusted to approximately 9.0 with 1.0 M imidazole and 0.5 M HCl. Subsequently, 0.4 g of cadmium powder was added to the solution and oscillated over night at 37 °C to completely reduce NO_3^- to NO_2^-. The reduction rate of NO_3^- was determined to be 98.33 ± 6.65% (n = 120). After standing for 30 min, 4 mL of the supernatant was transferred to a serum vial and crimp-sealed with a butyl rubber septum. Then, 0.2 mL of sodium azide (1:1 ratio of 20% acetic acid and 2 M sodium azide and purged with helium at 70 mL min⁻¹ for 10 min) was injected into the serum vial
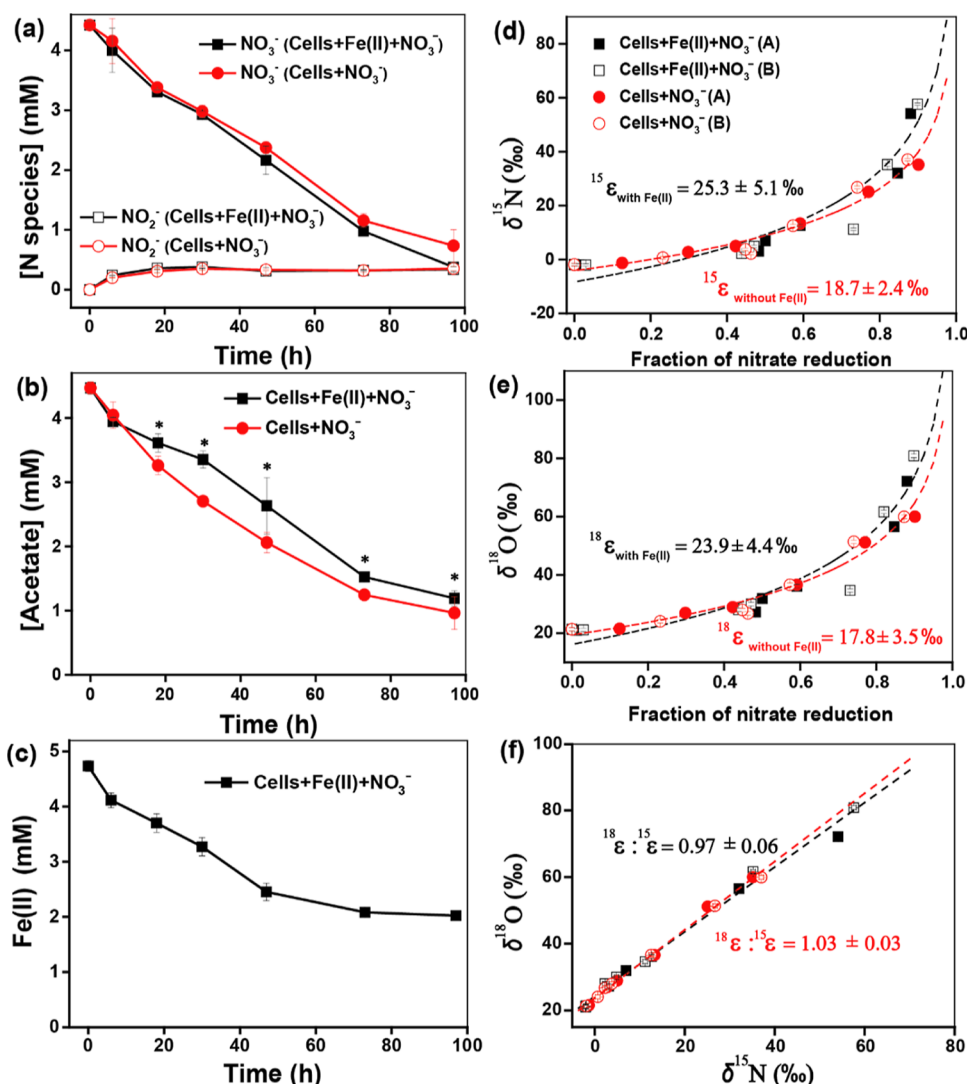
Figure 1. Change in concentrations of NO_3^- and NO_2^- (a), acetate (b), and Fe(II) (c) in cells + Fe(II) + NO_3^- and cells + NO_3^- treatments. Change in $\delta^{15}N–NO_3^-$ (d) and $\delta^{18}O–NO_3^-$ (e) to plotted vs change in fraction of nitrate reduction and (f) change in $\delta^{18}O–NO_3^-$ to plotted vs change in $\delta^{15}N–NO_3^-$ in cells + Fe(II) + NO_3^- and cells + NO_3^- treatments. The symbol * in panel (b) indicates a significant difference in the concentration of acetate in these two treatments, statistically analyzed by the T-test.

Table 1. Rate Constants, $^{15}\varepsilon$ Values, $^{18}\varepsilon$ Values, and Ratios of $^{18}\varepsilon$:$^{15}\varepsilon$ for Nitrate and Nitrite Reduction

	pseudo-first-order rate constant (k, h^{-1})		$^{15}\varepsilon$ (‰)	$^{18}\varepsilon$ (‰)	$^{18}\varepsilon/^{15}\varepsilon$
treatments	NO_3^-	NO_2^-			
cells + NO_3^-	0.013 ± 0.001		18.7 ± 2.4	17.8 ± 3.5	1.03 ± 0.03
cells + Fe(II) + NO_3^-	0.015 ± 0.001		25.3 ± 5.1	23.9 ± 4.4	0.97 ± 0.06
Fe(II) + NO_2^-		0.014 ± 0.001	23.2 ± 1.6	13.4 ± 0.7	0.58 ± 0.05
cells + NO_2^-		0.057 ± 0.006	15.4 ± 0.7	−6.4 ± 1.7	−0.41 ± 0.11
cells + Fe(II) + NO_2^-		0.015 ± 0.001	20.2 ± 1.5	14.3 ± 1.9	0.70 ± 0.08

with a microsyringe to reduce NO_2^- to N_2O. After 2 h, the reaction was stopped by adding 0.4 mL of 10 M NaOH. The $\delta^{15}N$ and $\delta^{18}O$ values of N_2O were measured by an isotope ratio mass spectrometer (MAT253, Thermo Fisher Scientific, Waltham, MA, USA). Mixtures of USGS34 and USGS32 with five different volume ratios (5:1, 4:2, 3:3, 2:4, and 1:5) were used as standards to calibrate the $\delta^{15}N$ values of the nitrate and nitrite samples. The correlation curve between the known isotopic compositions of NO_3^- and the measured isotopic compositions of N_2O was provided in Figure S1. N and O isotope fractionation was demonstrated not to occur during the

first step of NO_3^- reduction to NO_2^-.[26] All the standards were measured three times. The external reproducibility of the isotopic analyses was within ±0.5‰ for $\delta^{15}N$ and ±0.6‰ for $\delta^{18}O$.

2.4. Notation. The isotope fractionation factor α (where $\alpha = R_{reactant}/R_{product}$) was utilized to determine the magnitude of fractionation between the reactant and product. The value of α during nitrate and nitrite reduction was determined via the Rayleigh fractionation model as follows

$$\delta_t = (\delta_o + 1000)f^{\alpha-1} - 1000 \tag{1}$$

where δ_o and δ_t are the isotopic composition at the start and at time t afterward of each experiment, respectively, and f is the residual nitrate or nitrite fraction. The value of α can be converted into the isotope enrichment factor ε as follows

$$\varepsilon = (\alpha - 1) \times 1000 \qquad (2)$$

The value and 95% confidence interval of ε were determined by performing linear regression of the data in $\ln[(\delta_t + 1000)/(\delta_0 + 1000)]$ vs $\ln(f)$ space using Isoplot (version 4.15).[8]

3. RESULTS

3.1. Nitrate Reduction and Fe(II) Oxidation by Strain BoFeN1 with or without Fe(II). With or without Fe(II), the kinetics of nitrate reduction by strain BoFeN1 were similar (Figure 1a) and values of the rate constants (k) were 0.015 ± 0.001 h^{-1} ($R^2 = 0.991$) and 0.013 ± 0.001 h^{-1} ($R^2 = 0.994$), respectively (Table 1). The intermediate products of nitrate reduction with and without Fe(II) were measured. No NH$_4^+$ was detected, and the concentrations of the produced nitrite were 0.34 and 0.35 mM with or without Fe(II), respectively (Figure 1a). In the presence and absence of Fe(II), the k values during acetate oxidation were 0.014 ± 0.001 h^{-1} ($R^2 = 0.974$) and 0.016 ± 0.001 h^{-1} ($R^2 = 0.994$), respectively (Figure 1c). A t-test was used to statistically analyze the concentration of acetate in the two treatments. The acetate consumption with Fe(II) was significantly lower than that without Fe(II).

The concentration of Fe(II) decreased from 4.7 to 2.0 mM within 97 h (Figure 1c). Using XRD, we identified the Fe(III) mineral produced as lepidocrocite (Figure S2). To investigate the microbe-mineral associations in the strain BoFeN1, samples collected after 10, 30, and 80 h were thin-sectioned and analyzed by TEM. The minerals had needle- and rod-like shapes. The TEM results showed that free precipitates were present as well as closely associated precipitates with the cells covering their exterior during NRFO (Figure S3a−c). Therefore, the minerals formed can be mainly divided into two types: encrusting the cells (red arrows in Figure S3) and another that was formed at a distance from the cells (black arrows in Figure S3). With increasing Fe(II) oxidation, cell encrustation became more evident, and the crystal structures of the minerals away from the cells became more obvious, for example, by the formation of needle-like minerals at 80 h (Figure 2c).

3.2. N and O Isotope Effect of Nitrate Reduction. The values of δ^{15}N−NO$_3^-$ and δ^{18}O−NO$_3^-$ in the remaining nitrate followed a Rayleigh fractionation trend and increased as nitrate reduction proceeded, with or without Fe(II). With Fe(II), the values of δ^{15}N−NO$_3^-$ increased from −1.9 to 55.9‰ with 91% nitrate reduction, whereas without Fe(II), they increased from −1.9 to 36.1‰ with 84% nitrate reduction (Figure 1d). During nitrate reduction with or without Fe(II), the values of $^{15}\varepsilon$-NO$_3^-$ were 25.3 ± 5.1 and 18.7 ± 2.4‰, respectively, indicating similar $^{15}\varepsilon$-NO$_3^-$ values for these two treatments. The values of $^{18}\varepsilon$-NO$_3^-$, with or without Fe(II), were 23.9 ± 4.4 and 17.8 ± 3.5‰, respectively (Figure 1e). The ratios of ($^{18}\varepsilon$:$^{15}\varepsilon$)-NO$_3^-$, with or without Fe(II), were 0.97 ± 0.06 and 1.03 ± 0.03, respectively (Figure 1f).

3.3. Nitrite Reduction and Fe(II) Oxidation during Chemodenitrification, Microbial Nitrite Reduction, and the Coupled Process. The k value of nitrite reduction was 0.014 ± 0.001 h^{-1} ($R^2 = 0.971$) during chemodenitrification (NO$_2^-$ + Fe(II)) (Table 1 and Figure 2a). The k values during microbial nitrite reduction (cells + NO$_2^-$) and the coupled

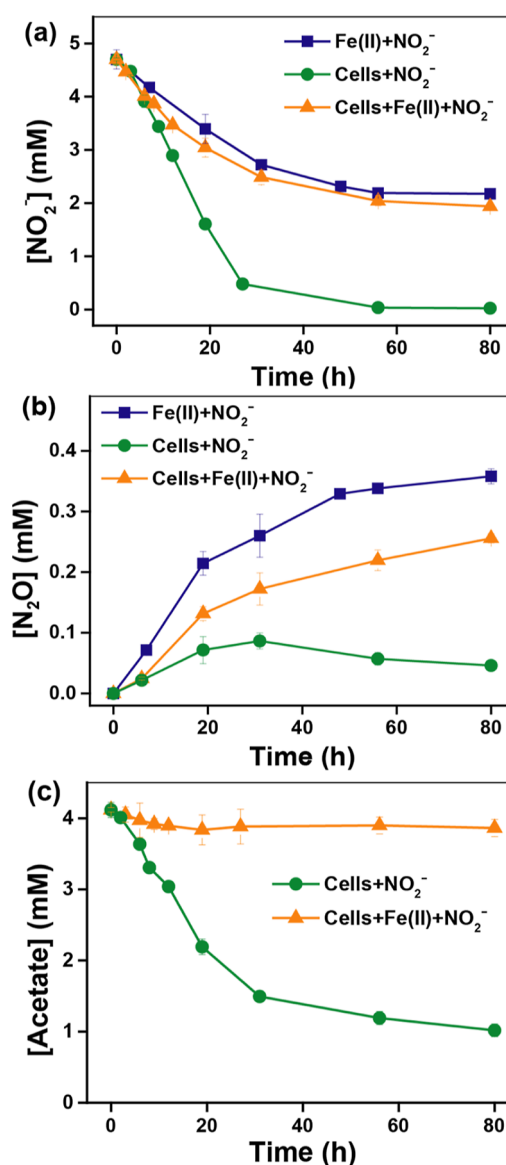**Figure 2.** Kinetic results of nitrite reduction (a), N$_2$O formation (b), and acetate consumption (c) in the Fe(II) + NO$_2^-$, cells + NO$_2^-$, and cells + Fe(II) + NO$_2^-$ treatments.

process [cells + NO$_2^-$ + Fe(II)] were 0.057 ± 0.006 h^{-1} ($R^2 = 0.935$) and 0.015 ± 0.001 h^{-1} ($R^2 = 0.936$), respectively (Table 1 and Figure 2a). No NH$_4^+$ was detected. N$_2$O was measured as a nitrite reduction product. The production of N$_2$O by the coupled process was 0.26 mM at 80 h, which was higher than that by the microbial process (0.05 mM) (Figure 2b). NO is unstable and difficult to measure, whereas N$_2$ was used as inert gas to replace O$_2$ in the serum bottle. Therefore, NO and N$_2$ were not measured in this study. The acetate of 3.1 mM was oxidized during the biological process, whereas only 0.26 mM acetate was consumed during the coupled process (Figure 2c).

The k values of Fe(II) oxidation during chemodenitrification and the coupled processes were 0.014 ± 0.001 h^{-1} ($R^2 = 0.971$) and 0.015 ± 0.001 h^{-1} ($R^2 = 0.936$), respectively (Figure 3a). The XRD results showed that the primary mineral in both treatments was lepidocrocite (Figure 3b). Scanning electron microscopy (SEM) analyses of the chemodenitrification setup showed the formation of rod-like lepidocrocite
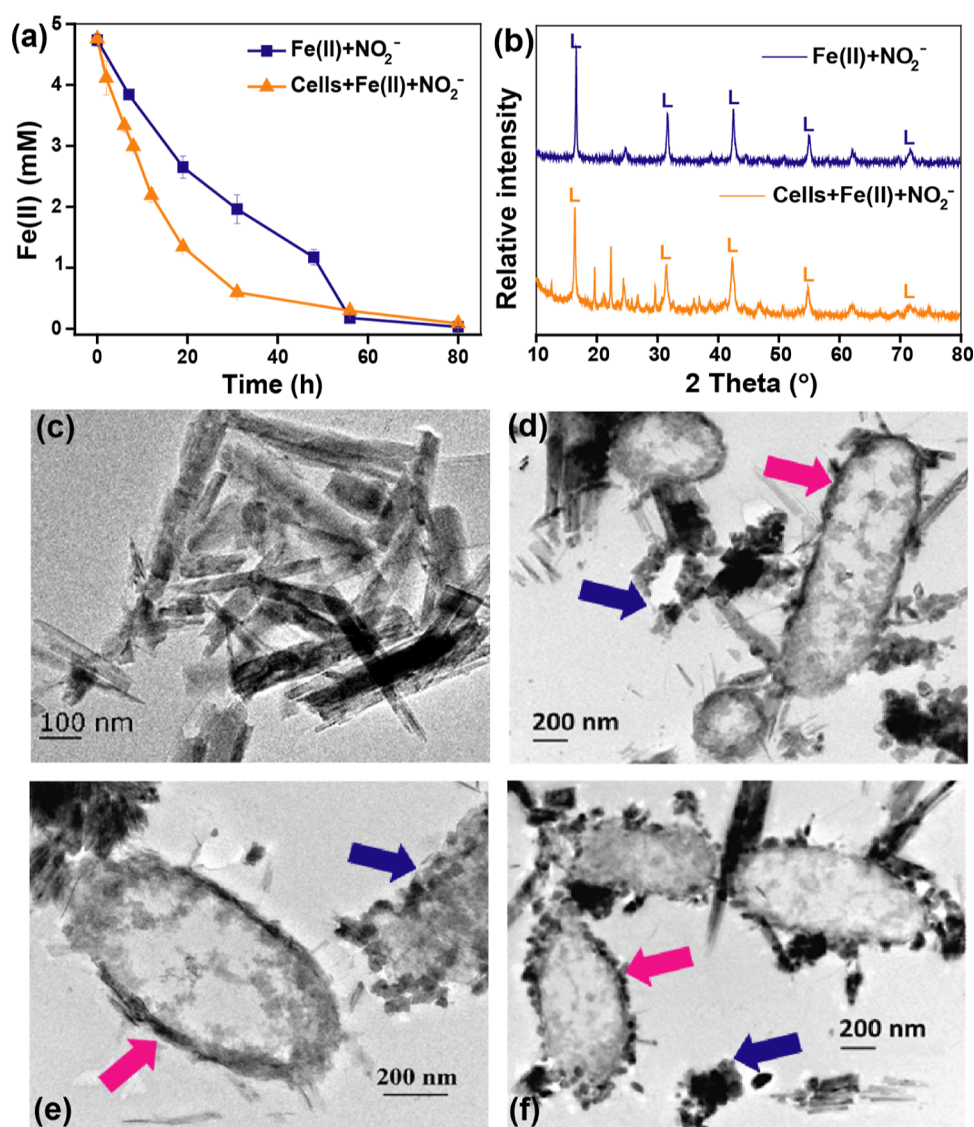
Figure 3. Kinetic results of Fe(II) oxidation (a) and XRD patterns of Fe(III) minerals (b) in the treatments of $[Fe(II) + NO_2^-]$ and $[cells + Fe(II) + NO_2^-]$. "L" stands for lepidocrocite. (c) SEM image of Fe(III) minerals in the treatment of $[Fe(II) + NO_2^-]$; (d−f) TEM images of transversal section of the strain BoFeN1 in $[cells + Fe(II) + NO_2^-]$ treatment at 10, 30, and 80 h. The blue arrows were used to point out the Fe(III) minerals presented at a distance to the cells, whereas magenta arrows were used to point out the Fe(III) minerals attached to the cell surface.

(Figure 3c), which was similar to the minerals formed during NRFO by the strain BoFeN1. The results of TEM images at 10, 30, and 80 h during the coupled processes show that a fraction of the Fe(III) minerals formed was present at a distance to the cells (blue arrows in Figure 3d−f), whereas the other fraction was attached to the surface of the cells (magenta arrows in Figure 3d−f). Compared to cell encrustation during NRFO by strain BoFeN1, many uncovered parts of the cells were observed during the coupled process. Fe(III) minerals covering the surface of the cells during NRFO by strain BoFeN1 appeared tighter than those formed during the coupled process.

3.4. N and O Isotope Fractionation during Chemo-denitrification, Microbial Nitrite Reduction, and the Coupled Process. The N−O isotope fractionation of the remaining nitrite for the chemical $[NO_2^- + Fe(II)]$, microbial (cells + NO_2^-), and coupled $[cells + NO_2^- + Fe(II)]$ processes was investigated. For the chemical process, the values of $\delta^{15}N-NO_2^-$ increased from 0.8 to 19.1‰ and the values of $\delta^{18}O-$

NO_2^- increased from 6.0 to 15.7‰ with 53% of nitrite reduction (Figure 4a,b). The values of $^{15}\varepsilon$-NO_2^- and $^{18}\varepsilon$-NO_2^- were 23.2 ± 1.6 and 13.4 ± 0.7‰, respectively. For the microbial process, $\delta^{15}N-NO_2^-$ values increased from 1.0 to 17.7‰ and the value of $^{15}\varepsilon$-NO_2^- was 15.4 ± 0.7‰. The values of $\delta^{18}O-NO_2^-$ decreased from 5.5 to −1.0 with 65% of nitrite reduction (Figure 4a,b). The corresponding $^{18}\varepsilon$-NO_2^- value was −6.4 ± 1.7‰. For the coupled process, $\delta^{15}N-NO_2^-$ increased from 1.0 to 13.3‰ and $\delta^{18}O-NO_2^-$ increased from 6.1 to 14.5‰ with 60% of nitrite reduction (Figure 4a,b). The $^{15}\varepsilon$-NO_2^- and $^{18}\varepsilon$-NO_2^- values during the coupled processes were 20.2 ± 1.5 and 14.3 ± 1.9‰, respectively (Figure 4a,b), which were similar to the $^{15}\varepsilon$-NO_2^- and $^{18}\varepsilon$-NO_2^- values during chemical nitrite reduction. The ratios of $(^{18}\varepsilon:^{15}\varepsilon)$-$NO_2^-$ were −0.41 ± 0.11 and 0.58 ± 0.05 during microbial and chemical nitrite reduction, respectively (Figure 4c). The ratio of $(^{18}\varepsilon:^{15}\varepsilon)$-$NO_2^-$ was 0.70 ± 0.08 during the coupled process, which was comparable to that observed in chemical nitrite reduction.
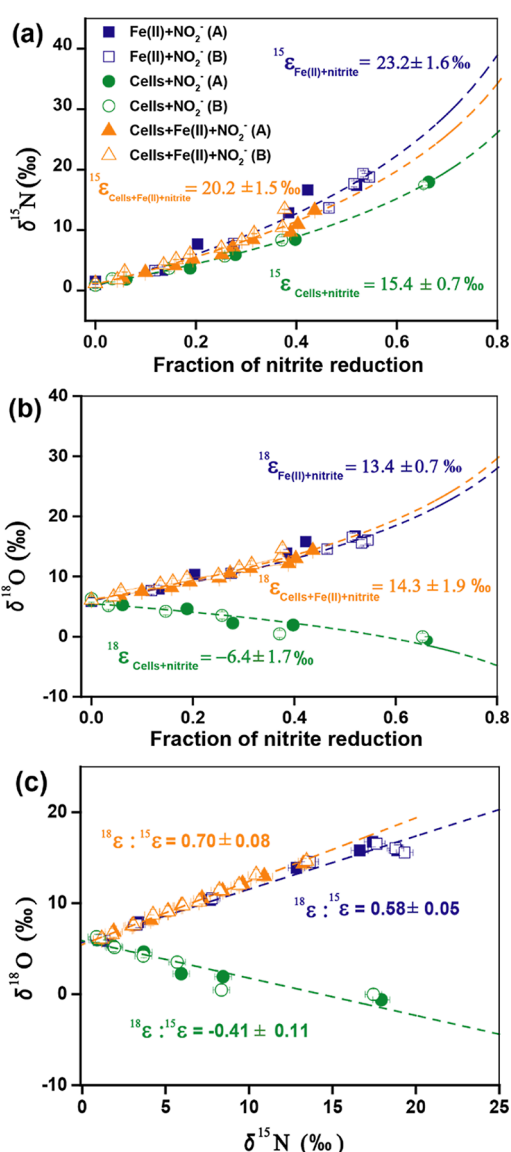
Figure 4. (a) δ^{15}N−NO$_2^-$ plotted vs fraction of nitrite reduction; (b) δ^{18}O−NO$_2^-$ plotted vs fraction of nitrite reduction; and (c) ratios of δ^{18}O−NO$_2^-$ to δ^{15}N−NO$_2^-$ in the [Fe(II) + NO$_2^-$], (cells + NO$_2^-$), and [cells + Fe(II) + NO$_2^-$] treatments.

4. DISCUSSION

4.1. Identifying Nitrate Reductase by the Ratio of ($^{18}\varepsilon$:$^{15}\varepsilon$)-NO$_3^-$.

In this study, with or without Fe(II), the ($^{18}\varepsilon$:$^{15}\varepsilon$)-NO$_3^-$ ratio during nitrate reduction by strain BoFeN1 was approximately 1.0, indicating that the main nitrate reductase functioning in strain BoFeN1 was Nar. The catalytic site of this enzyme is oriented toward the cytoplasm and releases protons into the periplasm thus directly contributing to energy conservation through the proton motive force.[27] Therefore, during NRFO by strain BoFeN1, nitrate was probably transferred from the exterior of the cells via the periplasm to the cytoplasm and then reduced to nitrite by Nar.

Irreversible N−O bond cleavage is sensitively isotopic step and results in the intrinsic $^{15}\varepsilon$-NO$_3^-$ during nitrate reduction. The mass-transfer steps during NRFO by strain BoFeN1 include all the steps before bond breakage. The mass-transfer steps are insensitively isotopic steps and cause little N isotope

effect (less than 2‰).[12] However, when the mass transfer becomes rate-limiting, the observed $^{15}\varepsilon$-NO$_3^-$ is suppressed, which is the "masking effect". During NRFO by the strain 2002, the ratios of ($^{18}\varepsilon$:$^{15}\varepsilon$)-NO$_3^-$ were 0.50−0.73, which were distinct from those by strain BoFeN1.[7] The distinct ratios of ($^{18}\varepsilon$:$^{15}\varepsilon$)-NO$_3^-$ during NRFO for these two strains were probably caused by different nitrate reductases (Nar vs Nap). Nar and Nap differ in their binding affinities and reducing activities, resulting in different effects on isotope fractionation.[7] Binding to Nar had a comparable masking effect on N and O isotope fractionation, leading to an ($^{18}\varepsilon$:$^{15}\varepsilon$)-NO$_3^-$ ratio of approximately 1.0. The O isotope effect may become more sensitive than that of N isotope to the mass-transfer limitation during NRFO by Nap, resulting in an ($^{18}\varepsilon$:$^{15}\varepsilon$)-NO$_3^-$ ratio of 0.4−0.7. Compared to conventional 16S sequencing measurements, dual N−O isotopes have the advantage of identifying and quantifying relevant nitrate reductase, which is truly expressed and functional during nitrate transformation in the environment. Additionally, the relative contribution of nitrate dissimilatory reduction between Nar and Nap can be evaluated by N−O isotopes in systems where both reductases are expressed.

Cell encrustation had no significant effect on isotope fractionation during NRFO by the strain BoFeN1. Cell encrustation was obvious after 10 h of reaction. Cell encrustation might induce the damage of cellular metabolic systems.[28] The similar rate of nitrate reduction and nitrite formation during NRFO in this study indicates that strain BoFeN1 was still metabolically active after cell encrustation. Rapid nitrate reduction and acetate consumption were still observed, which was consistent with the results of Klueglein et al. (2014).[17] Based on experiments with ^{13}C-acetate, non- and moderately mineralized cells were able to assimilate acetate, whereas completely mineralized cells prevented any carbon incorporation.[16] Secretion of EPS by strain BoFeN1 was suggested to be a defense mechanism against cell encrustation and a detoxification mechanism for Fe(II).[17,29,30] EPS contains polysaccharides, proteins, and lipids, which can inhibit the formation of larger mineral crystals within the EPS layer.[31] A large amount of EPS was produced only when strain BoFeN1 was cultured in the presence of Fe(II), which might protect cells from cell encrustation and then result in similar kinetics with nitrate reduction in the absence of Fe(II).[29] Similar isotope fractionation, with or without Fe(II), indicated that cell encrustation during NRFO by strain BoFeN1 probably did not result in additional nitrate-transfer limitations. Treibergs and Granger (2017) measured the values of $^{15}\varepsilon$-NO$_3^-$ during nitrate reduction by purified Nar extracts.[13] Nar with artificial viologen electron donors during nitrate reduction induced $^{15}\varepsilon$-NO$_3^-$ of 28‰, whereas the values of $^{15}\varepsilon$-NO$_3^-$ during nitrate reduction by Nar fueled with the physiological reductant hydroquinone was up to 33‰. The mass-transfer processes during nitrate reduction by strain BoFeN1 are diffusion, uptake of nitrate through the cell membrane, and binding to Nar, whereas that by purified Nar extracts is binding to Nar. Therefore, the masking effect during nitrate reduction by purified Nar extracts was weaker than that by strain BoFeN1 and the $^{15}\varepsilon$-NO$_2^-$ value induced by purified Nar extracts was more close to intrinsic $^{15}\varepsilon$-NO$_3^-$.

4.2. Distinguishing Chemical from Microbial Nitrite Reduction by Isotope Fractionation.

The $^{15}\varepsilon$-NO$_2^-$ value of chemical nitrite reduction (23.2 ± 1.6‰) was substantially higher than the $^{15}\varepsilon$-NO$_2^-$ value of microbial nitrite reduction
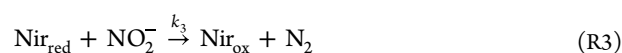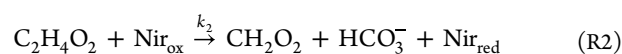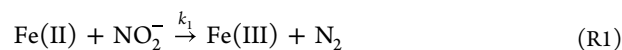
(15.4 ± 0.7‰). The nitrite-transfer step during chemical nitrite reduction is diffusion, whereas the nitrite-transfer steps during microbial nitrite reduction are diffusion, uptake of nitrite across the cell membrane, and binding to nitrite reductase.[8,20] Therefore, mass transfer during microbial nitrite reduction involves multiple processes, related to the process of chemical reduction by Fe(II). The masking effect resulted from the nitrite-transfer steps during chemical nitrite reduction was weaker than those observed during bacterial nitrite reduction, resulting in a higher $^{15}\varepsilon$-NO$_2^-$ value.[8] The O isotope fractionation of chemodenitrification followed a normal Rayleigh fractionation trend with the $^{18}\varepsilon$-NO$_2^-$ value of 13.4 ± 0.7‰, whereas that during microbial nitrite reduction followed an inverse Rayleigh fractionation trend with the $^{18}\varepsilon$-NO$_2^-$ value of −6.4 ± 1.7‰. During microbial nitrite reduction, O isotope fractionation probably results from the combined effects of kinetic isotope fractionation and O atom exchange between nitrite and water.[20,21,32] The isotope fractionation of microbial nitrite reduction indicated that O atom exchange between nitrite and water plays more important roles in controlling isotope fractionation than those for chemodenitrification. At pH 7.0, the equilibration of O isotopes between nitrite and water will occur. However, because these experiments occurred over a course of several days, the abiotic isotopic equilibrium is too slow and not likely relevant. Instead, it is possible that an enzyme-mediated equilibrium is at work. The strain BoFeN1 harbors genes that express both nitrite reductase (NirS and NirK).[33] The strain BoFeN1 appears to exhibit some sort of physiological impact arising from the presence of nitrite, which is toxic to the bacteria. Under such stress, NirS and/or NirK are known to exhibit some degree of reversibility and this may lead to the ingrowth of water O atom exchange between nitrite and water.

Furthermore, the ratio of ($^{18}\varepsilon$:$^{15}\varepsilon$)-NO$_2^-$ was 0.58 ± 0.05 during chemical nitrite reduction, which was substantially distinct from that during microbial nitrite reduction, indicating that N and O isotopes are promising methods for differentiating microbial reduction from chemical reduction under comparable environmental conditions. During microbial nitrate/nitrite reduction, although $^{15}\varepsilon$ and $^{18}\varepsilon$ may change with various experimental effects (e.g., nitrate/nitrite concentrations and carbon source concentrations), the kinetic isotope effect of N and O was masked to the same extent, and isotope effects changed synchronously. Thus, the ratios of $^{18}\varepsilon$:$^{15}\varepsilon$ remained unchanged under different experimental conditions.[7,12-15,20,34] The ratios of $^{18}\varepsilon$:$^{15}\varepsilon$ depend on the type of reductase. These results indicate that the slopes in the dual N and O isotope plots were much less affected by mass-transfer limitations than those of single N or O isotopes. During chemical nitrite reduction, changes of nitrite concentration unlikely affected the ratios of ($^{18}\varepsilon$:$^{15}\varepsilon$)-NO$_2^-$. Buchwald et al. (2016)[21] found that when the pH was 7.0, the initial concentrations of Fe(II) and nitrite were 4.7 and 0.2 mM, respectively, and that of ($^{18}\varepsilon$:$^{15}\varepsilon$)-NO$_2^-$ was 0.7. In this study, the initial nitrite concentration was much higher (4.7 mM) and other experimental parameters [the pH of 7.0 and the initial Fe(II) concentration of 4.7 mM] were similar. The corresponding ($^{18}\varepsilon$:$^{15}\varepsilon$)-NO$_2^-$ was 0.58 ± 0.05, which was similar with that from Buchwald et al. (2016).[21] It was not only because similar ratios of ($^{18}\varepsilon$:$^{15}\varepsilon$)-NO$_2^-$ between chemical nitrite reduction and the coupled process, but also because the ratios of ($^{18}\varepsilon$:$^{15}\varepsilon$)-NO$_2^-$ during chemical nitrite reduction and the coupled process were positive and that during microbial

nitrite reduction was negative. Thus, even if ratios of ($^{18}\varepsilon$:$^{15}\varepsilon$)-NO$_2^-$ change to some extent with various experimental factors, the directions of Rayleigh fractionation trend during N and O isotope fractionation are unlikely to change. Therefore, a similar conclusion of the contribution of chemodenitrification and biological reactions to the coupled process at different concentrations of electrolyte was likely to obtain. The reaction between the produced ammonium and the generated Fe(III) was also unlikely to occur. No NH$_4^+$ was detected during nitrate and nitrite reduction in this study. Even if NH$_4^+$ existed in this system, NH$_4^+$ could not chemically react with the generated Fe(III).[35] Furthermore, it was demonstrated that Fe(III) could not be reduced by strain BoFeN1 with acetate as the electron donor.[28]

The ratio of ($^{18}\varepsilon$:$^{15}\varepsilon$)-NO$_2^-$ was 0.70 ± 0.08 during the coupled process [cells + NO$_2^-$ + Fe(II)]. The $^{15}\varepsilon$-NO$_2^-$ value, $^{18}\varepsilon$-NO$_2^-$ value, and ratio of ($^{18}\varepsilon$:$^{15}\varepsilon$)-NO$_2^-$ during the coupled processes were similar to those during chemical nitrite reduction and substantially different from microbial nitrite reduction, indicating that chemical nitrite reduction was the major process during the coupled processes. In contrast, an elementary-reaction-based kinetic model revealed that the relative contribution of microbial nitrite reduction was higher than that of chemical reduction.[19] The different results between this study and that of Liu et al. (2019)[19] are because the relative contribution of microbial and chemical nitrite reduction was evaluated during nitrate reduction in the presence of Fe(II) and strain BoFeN1 [cells + NO$_3^-$ + Fe(II)] in the study of Liu et al. (2019),[19] whereas the treatment was cells + NO$_2^-$ + Fe(II) in this study. Nitrate is reduced to nitrite by Nar in the cytoplasmic membrane, and nitrite can be directly reduced by NirK and/or NirS. With continuous consumption of nitrite, the nitrite concentration remained low in the treatment of [cells + NO$_3^-$ + Fe(II)]. In this study, biological and chemical nitrite reduction was distinguished during nitrite reduction with Fe(II) and strain BoFeN1 [cells + NO$_2^-$ + Fe(II)]. The nitrite concentration was much higher, and nitrite directly reacted with Fe(II).

4.3. Kinetic Model of Chemical and Microbial Nitrite Reduction. To further reveal the relative contribution of chemical and microbial nitrite reduction during the coupled process [cells + NO$_2^-$ + Fe(II)], a kinetic model was established. For chemical nitrite reduction, nitrite was reduced by Fe(II) (R1). For microbial reduction, acetate serves as the electron donor and oxidized nitrite reductase (Nir$_{ox}$) was changed to reduced nitrite reductase (Nir$_{red}$) (R2). Nitrite was microbially reduced by Nir$_{red}$ (R3). During the coupled process, nitrite was chemically reduced by Fe(II) with Fe(II) oxidation (R1), whereas it could also be microbially reduced by Nir$_{red}$ (R2 and R3). The equations of all elementary reactions during chemical reduction, microbial reduction, and the coupled process are represented as follows

$$\text{Fe(II)} + \text{NO}_2^- \xrightarrow{k_1} \text{Fe(III)} + \text{N}_2 \tag{R1}$$

$$\text{C}_2\text{H}_4\text{O}_2 + \text{Nir}_{ox} \xrightarrow{k_2} \text{CH}_2\text{O}_2 + \text{HCO}_3^- + \text{Nir}_{red} \tag{R2}$$

$$\text{Nir}_{red} + \text{NO}_2^- \xrightarrow{k_3} \text{Nir}_{ox} + \text{N}_2 \tag{R3}$$

The rate constants of R1−R3 are denoted as k_1, k_2, and k_3 (Table 2). The rate constants of R1−R3 were quantified by fitting experimental data with the model. The kinetic models for the [cells + Fe(II) + NO$_2^-$] treatments were developed in

Table 2. k Values for Elementary Reactions Derived from Kinetic Models in the Fe(II) + NO$_2^-$, Cells + NO$_2^-$, and Cells + Fe(II) + NO$_2^-$ Treatments

no	Fe(II) + NO$_2^-$ ($\times 10^{-3}$ nmol^{-1} L h^{-1})	cells + NO$_2^-$ ($\times 10^{-3}$ nmol^{-1} L h^{-1})	cells + Fe(II) + NO$_2^-$ ($\times 10^{-3}$ nmol^{-1} L h^{-1})
R1	8.9		14
R2		38.5	2.2
R3		342	0.1

accordance with R1−R3. The values of k_1−k_3 during the coupled process are listed in Table 2. The model-fitted kinetics of nitrite reduction, Fe(II) oxidation, and acetate consumptions are shown in Figure S4. The values of k_1 and k_3 during the coupled process were 14×10^{-3} and 0.1×10^{-3} nmol^{-1} L h^{-1}, respectively. The relative contributions for chemical and microbial reduction during the coupled process can be obtained from the values of k_1 and k_3. The relative contribution for chemical reduction was 99.3% during the coupled process, indicating that the chemical reduction is dominant during the coupled process. These results of kinetic modeling were consistent with those of isotope fractionation.

The k_2 values were 38.5×10^{-3} and 2.2×10^{-3} nmol^{-1} L h^{-1} in the treatment of (cells + NO$_2^-$) and [cells + NO$_2^-$ + Fe(II)], respectively. Moreover, the k_3 value in the treatment of (cells + NO$_2^-$) (342×10^{-3} nmol^{-1} L h^{-1}) was much higher than that in the treatment of [cells + NO$_2^-$ + Fe(II)] (0.1×10^{-3} nmol^{-1} L h^{-1}]. These results indicated that reduction rate of nitrite and consumption rate of acetate were pronouncedly suppressed in the presence of Fe(II). In the treatment of [cells + NO$_2^-$ + Fe(II)], Fe(II) may be rapidly and directly oxidized by nitrite and did not stimulate cells to secrete EPS. Therefore, strain BoFeN1 lost the protection of EPS and cell encrustation produced by Fe(III) minerals, resulting in the pronounced suppression of nitrite reduction, acetate consumption, and cellular metabolic activity. In the [cells + NO$_3^-$ + Fe(II)] treatment, nitrite is produced from nitrate reduction in the cytoplasm, transferred to the periplasm and exterior of the cells, and reacted with Fe(II). The nitrite concentration remained low (less than 0.4 mM), and the consumption rate of acetate stayed relatively high. The morphology of the minerals encrusted on the cell surface in the treatments of [cells + NO$_2^-$ + Fe(II)] and [cells + NO$_3^-$ + Fe(II)] was different. Compared to those in the [cells + NO$_2^-$ + Fe(II)] treatment (magenta arrows in Figure 3d−f), more minerals were homogeneously encrusted around the cells and formed complete cell encrustation on the cell surface (red arrows in Figure S3). In previous studies, the nitrite concentration was higher (1 mM) in the treatment of [strain 2002 + NO$_3^-$ + Fe(II)] than those in the treatment of [strain BoFeN1 + NO$_3^-$ + Fe(II)] in this study. The consumption rate of acetate and nitrate reduction rates was much lower in the [cells + NO$_3^-$ + Fe(II)] treatment than those in the treatment of (cells + NO$_3^-$).[7] These results also indicated that the accumulation of nitrite suppressed the secretion of EPS and metabolic activity of the cells. The genes of strain BoFeN1 encoding nitric oxide reductase (NorBC) were found in the genome of strain BoFeN1 (GCA_003345135.1). Thus, strain BoFeN1 is able to reduce NO into N$_2$O. The concentration of N$_2$O during microbial reduction was much lower than that during the coupled process. The pronounced suppression of N$_2$O reduction in the presence of Fe(II) was resulted from cell encrustation as well. The strain BoFeN1 harbors nosZ gene-

encoding N$_2$O reductase and was still able to reduce N$_2$O, whereas Fe(II) could only slightly reduce N$_2$O.[36] Therefore, the concentration of N$_2$O during microbial reduction was also much lower than that during chemdenitrification.

5. ENVIRONMENTAL IMPLICATIONS

Microbially mediated NRFO contributes to Fe and N biogeochemical cycling within a variety of submarine hydrothermal systems, wetland sediments, and paddy soil environments.[5] During NFRO, Fe(III) precipitates at circumneutral pH and highly sorptive and reactive surfaces to immobilize heavy metals. This offers extremely sorptive and reactive surfaces to immobile heavy metals.[2] During NRFO, nitrate is reduced to nitrite, and nitrite is further biologically reduced via NirS and/or NirK and chemically reduced by Fe(II). Distinguishing chemical reactions from biological reactions are still a big challenge.[37] This study demonstrated that biological and chemical nitrite reduction can be clearly distinguished by N−O isotopes and that the chemical reactions were dominant during the coupled process. Compared with kinetic modeling approaches, isotope fractionation provides direct experimental evidence to distinguish biological reactions from chemical reactions. The N and O isotopes can be applied to other analogous systems with the coexistence of chemical and biological processes. Furthermore, the strain BoFeN1 in this study was identified as an NRFO model bacterium. Actually, a large amount of bacteria have the ability to reduce nitrate to nitrite, which can chemically oxidize Fe(II).[38,39] Therefore, NRFO could be triggered by many other widespread denitrification bacteria. The combination of N−O isotopes and kinetic modeling can provide a comprehensive understanding of the molecular mechanisms of microbially mediated NRFO.

■ ASSOCIATED CONTENT

Ⓢ Supporting Information

The Supporting Information is available free of charge at https://pubs.acs.org/doi/10.1021/acs.est.3c02329.

> N and O isotope conversion curve for N$_2$O and NO$_3^-$ standards; XRD patterns of the minerals formed by Fe(II) oxidation with strain BoFeN1 and nitrate; TEM images of strain BoFeN1 in the treatment of [cells + Fe(II) + NO$_3^-$] after 10, 30, and 80 h; model-fitted kinetics of nitrite reduction as a function of time in Fe(II) + NO$_2^-$, cells + NO$_2^-$, and cells + Fe(II) + NO$_2^-$ treatments; Fe(II) oxidation as a function of time in the Fe(II) + NO$_2^-$ and cells + Fe(II) + NO$_2^-$ treatments; and acetate consumption as a function of time in the cells + NO$_2^-$ and cells + Fe(II) + NO$_2^-$ treatments (PDF)

■ AUTHOR INFORMATION

Corresponding Author

    Guojun Chen − *National-Regional Joint Engineering Research Center for Soil Pollution Control and Remediation in South China, Guangdong Key Laboratory of Integrated Agroenvironmental Pollution Control and Management, Institute of Eco-environmental and Soil Sciences, Guangdong Academy of Sciences, Guangzhou 510650, China;* ⓞ orcid.org/0000-0003-3081-629X; Email: gjchen@soil.gd.cn

Authors

Dandan Chen − *National-Regional Joint Engineering Research Center for Soil Pollution Control and Remediation in South China, Guangdong Key Laboratory of Integrated Agroenvironmental Pollution Control and Management, Institute of Eco-environmental and Soil Sciences, Guangdong Academy of Sciences, Guangzhou 510650, China; School of Biological and Chemical Engineering, Panzhihua University, Panzhihua 6170000, China*

Kuan Cheng − *National-Regional Joint Engineering Research Center for Soil Pollution Control and Remediation in South China, Guangdong Key Laboratory of Integrated Agroenvironmental Pollution Control and Management, Institute of Eco-environmental and Soil Sciences, Guangdong Academy of Sciences, Guangzhou 510650, China*

Tongxu Liu − *National-Regional Joint Engineering Research Center for Soil Pollution Control and Remediation in South China, Guangdong Key Laboratory of Integrated Agroenvironmental Pollution Control and Management, Institute of Eco-environmental and Soil Sciences, Guangdong Academy of Sciences, Guangzhou 510650, China;* orcid.org/0000-0002-2348-3952

Andreas Kappler − *Geomicrobiology, Department of Geosciences, University of Tübingen, Tübingen 72076, Germany; Cluster of Excellence: EXC 2124: Controlling Microbes to Fight Infection, Tübingen 72074, Germany;* orcid.org/0000-0002-3558-9500

Xiaomin Li − *SCNU Environmental Research Institute, Guangdong Provincial Key Laboratory of Chemical Pollution and Environmental Safety & MOE Key Laboratory of Theoretical Chemistry of Environment, South China Normal University, Guangzhou 510006, China;* orcid.org/0000-0001-8718-2780

Raymond Jianxiong Zeng − *Fujian Provincial Key Laboratory of Soil Environmental Health and Regulation, College of Resources and Environment, Fujian Agriculture and Forestry University, Fuzhou, Fujian 350002, China;* orcid.org/0000-0003-3060-588X

Yang Yang − *National-Regional Joint Engineering Research Center for Soil Pollution Control and Remediation in South China, Guangdong Key Laboratory of Integrated Agroenvironmental Pollution Control and Management, Institute of Eco-environmental and Soil Sciences, Guangdong Academy of Sciences, Guangzhou 510650, China*

Fujun Yue − *Institute of Surface-Earth System Science, School of Earth System Science, Tianjin University, Tianjin 300072, China*

Shiwen Hu − *National-Regional Joint Engineering Research Center for Soil Pollution Control and Remediation in South China, Guangdong Key Laboratory of Integrated Agroenvironmental Pollution Control and Management, Institute of Eco-environmental and Soil Sciences, Guangdong Academy of Sciences, Guangzhou 510650, China;* orcid.org/0000-0002-6679-5868

Fang Cao − *Yale-NUIST Center on Atmospheric Environment, International Joint Laboratory on Climate and Environment Change (ILCEC), Nanjing University of Information Science & Technology, Nanjing 210044, China*

Fangbai Li − *National-Regional Joint Engineering Research Center for Soil Pollution Control and Remediation in South China, Guangdong Key Laboratory of Integrated Agroenvironmental Pollution Control and Management, Institute of Eco-environmental and Soil Sciences, Guangdong Academy of Sciences, Guangzhou 510650, China;* orcid.org/0000-0001-9027-9313

Complete contact information is available at:
https://pubs.acs.org/10.1021/acs.est.3c02329

Author Contributions

○D.C. and K.C. contributed equally to this paper.

Notes

The authors declare no competing financial interest.

■ REFERENCES

(1) Kappler, A.; Bryce, C.; Mansor, M.; Lueder, U.; Byrne, J. M.; Swanner, E. D. An evolving view on biogeochemical cycling of iron. *Nat. Rev. Microbiol.* **2021**, *19*, 360−374.

(2) Li, X.; Zhang, W.; Liu, T.; Chen, L.; Chen, P.; Li, F. Changes in the composition and diversity of microbial communities during anaerobic nitrate reduction and Fe (II) oxidation at circumneutral pH in paddy soil. *Soil Biol. Biochem.* **2016**, *94*, 70−79.

(3) Kappler, A.; Schink, B.; Newman, D. K. Fe (III) mineral formation and cell encrustation by the nitrate-dependent Fe (II)-oxidizer strain BoFeN1. *Geobiology* **2005**, *3*, 235−245.

(4) Dong, H.; Huang, L.; Zhao, L.; Zeng, Q.; Liu, X.; Sheng, Y.; Shi, L.; Wu, G.; Jiang, H.; Li, F.; Zhang, L.; Guo, D.; Li, G.; Hou, W.; Chen, H. A critical review of mineral−microbe interaction and co-evolution: mechanisms and applications. *Natl. Sci. Rev.* **2022**, *9*, nwac128.

(5) Liu, T.; Chen, D.; Li, X.; Li, F. Microbially mediated coupling of nitrate reduction and Fe(II) oxidation under anoxic conditions. *FEMS Microbiol. Ecol.* **2019**, *95*, fiz030.

(6) Song, X.; Wang, P.; Van Zwieten, L.; Bolan, N.; Wang, H.; Li, X.; Cheng, K.; Yang, Y.; Wang, M.; Liu, T.; Li, F. Towards a better understanding of the role of Fe cycling in soil for carbon stabilization and degradation. *Carbon Res.* **2022**, *1*, 5.

(7) Chen, G.; Chen, D.; Li, F.; Liu, T.; Zhao, Z.; Cao, F. Dual nitrogen-oxygen isotopic analysis and kinetic model for enzymatic nitrate reduction coupled with Fe(II) oxidation by Pseudogulbenkiania sp. strain 2002. *Chem. Geol.* **2020**, *534*, 119456.

(8) Chen, G.; Zhao, W.; Yang, Y.; Chen, D.; Wang, Y.; Li, F.; Zhao, Z.; Cao, F.; Liu, T. Chemodenitrification by Fe(II) and nitrite: Effects of temperature and dual NO isotope fractionation. *Chem. Geol.* **2021**, *575*, 120258.

(9) Visser, A.; Wankel, S.; Frey, C.; Kappler, A.; Lehmann, M. Unchanged nitrate and nitrite isotope fractionation during heterotrophic and Fe (II)-mixotrophic denitrification suggest a non-enzymatic link between denitrification and Fe (II) oxidation. *Front. Microbiol.* **2022**, *13*, 927475.

(10) Jones, L. C.; Peters, B.; Lezama Pacheco, J. S.; Casciotti, K. L.; Fendorf, S. Stable isotopes and iron oxide mineral products as markers of chemodenitrification. *Environ. Sci. Technol.* **2015**, *49*, 3444−3452.

(11) Mariotti, A.; Germon, J.; Hubert, P.; Kaiser, P.; Letolle, R.; Tardieux, A.; Tardieux, P. Experimental determination of nitrogen

kinetic isotope fractionation: some principles; illustration for the denitrification and nitrification processes. *Plant Soil* **1981**, *62*, 413−430.

(12) Granger, J.; Sigman, D. M.; Lehmann, M. F.; Tortell, P. D. Nitrogen and oxygen isotope fractionation during dissimilatory nitrate reduction by denitrifying bacteria. *Limnol. Oceanogr.* **2008**, *53*, 2533−2545.

(13) Treibergs, L. A.; Granger, J. Enzyme level N and O isotope effects of assimilatory and dissimilatory nitrate reduction. *Limnol. Oceanogr.* **2017**, *62*, 272−288.

(14) Asamoto, C. K.; Rempfert, K. R.; Luu, V. H.; Younkin, A. D.; Kopf, S. H. Enzyme-specific coupling of oxygen and nitrogen isotope fractionation of the Nap and Nar nitrate reductases. *Environ. Sci. Technol.* **2021**, *55*, 5537−5546.

(15) Frey, C.; Hietanen, S.; Jürgens, K.; Labrenz, M.; Voss, M. N and O isotope fractionation in nitrate during chemolithoautotrophic denitrification by Sulfurimonas gotlandica. *Environ. Sci. Technol.* **2014**, *48*, 13229−13237.

(16) Miot, J.; Remusat, L.; Duprat, E.; Gonzalez, A.; Pont, S.; Poinsot, M. Fe biomineralization mirrors individual metabolic activity in a nitrate-dependent Fe(II)-oxidizer. *Front. Microbiol.* **2015**, *6*, 879.

(17) Klueglein, N.; Zeitvogel, F.; Stierhof, Y.-D.; Floetenmeyer, M.; Konhauser, K. O.; Kappler, A.; Obst, M. Potential role of nitrite for abiotic Fe(II) oxidation and cell encrustation during nitrate reduction by denitrifying bacteria. *Appl. Environ. Microbiol.* **2014**, *80*, 1051−1061.

(18) Chen, D.; Liu, T.; Li, X.; Li, F.; Luo, X.; Wu, Y.; Wang, Y. Biological and chemical processes of microbially mediated nitrate-reducing Fe(II) oxidation by Pseudogulbenkiania sp. strain 2002. *Chem. Geol.* **2018**, *476*, 59−69.

(19) Liu, T.; Chen, D.; Luo, X.; Li, X.; Li, F. Microbially mediated nitrate-reducing Fe (II) oxidation: Quantification of chemodenitrification and biological reactions. *Geochem. Cosmochim. Acta* **2019**, *256*, 97−115.

(20) Martin, T. S.; Casciotti, K. L. Nitrogen and oxygen isotopic fractionation during microbial nitrite reduction. *Limnol. Oceanogr.* **2016**, *61*, 1134−1143.

(21) Buchwald, C.; Grabb, K.; Hansel, C. M.; Wankel, S. D. Constraining the role of iron in environmental nitrogen transformations: Dual stable isotope systematics of abiotic NO_2^- reduction by Fe(II) and its production of N_2O. *Geochem. Cosmochim. Acta* **2016**, *186*, 1−12.

(22) Grabb, K. C.; Buchwald, C.; Hansel, C.; Wankel, S. D. A dual nitrite isotopic investigation of chemodenitrification by mineral-associated Fe(II) and its production of nitrous oxide. *Geochim. Cosmochim. Acta* **2017**, *196*, 388−402.

(23) Visser, A. N.; Wankel, S. D.; Niklaus, P. A.; Byrne, J. M.; Kappler, A. A.; Lehmann, M. F. Impact of reactive surfaces on the abiotic reaction between nitrite and ferrous iron and associated nitrogen and oxygen isotope dynamics. *Biogeosci. Discuss.* **2020**, *17*, 4355−4374.

(24) Pantke, C.; Obst, M.; Benzerara, K.; Morin, G.; Ona-Nguema, G.; Dippon, U.; Kappler, A. Green rust formation during Fe(II) oxidation by the nitrate-reducing Acidovorax sp. strain BoFeN1. *Environ. Sci. Technol.* **2012**, *46*, 1439−1446.

(25) Li, X.; Hou, L.; Liu, M.; Zheng, Y.; Yin, G.; Lin, X.; Cheng, L.; Li, Y.; Hu, X. Evidence of nitrogen loss from anaerobic ammonium oxidation coupled with ferric iron reduction in an intertidal wetland. *Environ. Sci. Technol.* **2015**, *49*, 11560−11568.

(26) McIlvin, M. R.; Altabet, M. A. Chemical conversion of nitrate and nitrite to nitrous oxide for nitrogen and oxygen isotopic analysis in freshwater and seawater. *Anal. Chem.* **2005**, *77*, 5589−5595.

(27) Kuypers, M. M.; Marchant, H. K.; Kartal, B. The microbial nitrogen-cycling network. *Nat. Rev. Microbiol.* **2018**, *16*, 263−276.

(28) Muehe, E. M.; Gerhardt, S.; Schink, B.; Kappler, A. Ecophysiology and the energetic benefit of mixotrophic Fe(II) oxidation by various strains of nitratereducing bacteria. *FEMS Microbiol. Ecol.* **2009**, *70*, 335−343.

(29) Schmid, G.; Zeitvogel, F.; Hao, L.; Ingino, P.; Floetenmeyer, M.; Stierhof, Y.-D.; Schroeppel, B.; Burkhardt, C. J.; Kappler, A.; Obst, M. 3-D analysis of bacterial cell-(iron)mineral aggregates formed during Fe(II) oxidation by the nitrate-reducing Acidovorax sp. strain BoFeN1 using complementary microscopy tomography approaches. *Geobiology* **2014**, *12*, 340−361.

(30) Miot, J.; Maclellan, K.; Benzerara, K.; Boisset, N. Preservation of protein globules and peptidoglycan in the mineralized cell wall of nitrate-reducing, iron(II)-oxidizing bacteria: a cryo-electron microscopy study. *Geobiology* **2011**, *9*, 459−470.

(31) Hao, L.; Li, J.; Kappler, A.; Obst, M. Mapping of heavy metal ion sorption to cell-extracellular polymeric substance-mineral aggregates by using metal-selective fluorescent probes and confocal laser scanning microscopy. *Appl. Environ. Microbiol.* **2013**, *79*, 6524−6534.

(32) Casciotti, K. L.; Böhlke, J. K.; McIlvin, M. R.; Mroczkowski, S. J.; Hannon, J. E. Oxygen isotopes in nitrite: Analysis, calibration, and equilibration. *Anal. Chem.* **2007**, *79*, 2427−2436.

(33) Price, A.; Macey, M. C.; Miot, J.; Olsson-Francis, K. Draft genome sequences of the nitrate-dependent iron-oxidizing proteobacteria Acidovorax sp. strain BoFeN1 and Paracoccus pantotrophus strain KS1. *Microbiol. Resour. Announce.* **2018**, *7*, No. e01050.

(34) Sebilo, M.; Aloisi, G.; Mayer, B.; Perrin, E.; Vaury, V.; Mothet, A.; Laverman, A. M. Controls on the isotopic composition of nitrite ($\delta^{15}N$ and $\delta^{18}O$) during denitrification in freshwater sediments. *Sci. Rep.* **2019**, *9*, 19206.

(35) Zhou, G.-W.; Yang, X.-R.; Li, H.; Marshall, C. W.; Zheng, B.-X.; Yan, Y.; Su, J.-Q.; Zhu, Y.-G. Electron shuttles enhance anaerobic ammonium oxidation coupled to iron(III) reduction. *Environ. Sci. Technol.* **2016**, *50*, 9298−9307.

(36) Moraghan, J.; Buresh, R. Chemical reduction of nitrite and nitrous oxide by ferrous iron. *Soil Sci. Soc. Am. J.* **1977**, *41*, 47−50.

(37) Melton, E. D.; Swanner, E. D.; Behrens, S.; Schmidt, C.; Kappler, A. The interplay of microbially mediated and abiotic reactions in the biogeochemical Fe cycle. *Nat. Rev. Microbiol.* **2014**, *12*, 797−808.

(38) Kopf, S. H.; Henny, C.; Newman, D. K. Ligand-enhanced abiotic iron oxidation and the effects of chemical versus biological iron cycling in anoxic environments. *Environ. Sci. Technol.* **2013**, *47*, 2602−2611.

(39) Picardal, F. Abiotic and microbial interactions during anaerobic transformations of Fe(II) and NOx. *Front. Microbiol.* **2012**, *3*, 112.